Inorganic Chemistry Communications 178 (2025) 114426

Contents lists available at ScienceDirect

Inorganic Chemistry Communications

journal homepage: www.elsevier.com/locate/inoche

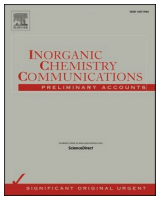

Research Article

The impact of metal ions on the photo-antibacterial efficiency of metalloporphyrins with triphenylphosphonium units

Inês Chaves [a], Filipe F.M. Morais [b], Cátia Vieira [a], Maria Bartolomeu [c], Ana T.P.C. Gomes [c], M. Amparo F. Faustino [b], M. Graça P.M.S. Neves [b], Adelaide Almeida [a,*], Nuno M.M. Moura [b,*]

[a] CESAM, Department of Biology, University of Aveiro, 3810-193 Aveiro, Portugal
[b] LAQV-REQUIMTE, Department of Chemistry, University of Aveiro, 3810-193 Aveiro, Portugal
[c] Universidade Católica Portuguesa, Faculdade de Medicina Dentária, Centro de Investigação Interdisciplinar em Saúde, 3504-505 Viseu, Portugal

ARTICLE INFO

Keywords:
Metalloporphyrin
Triphenylphosphonium
Zinc(II)
Antimicrobial photodynamic therapy
Photosensitizers
Bacteria

ABSTRACT

The influence of metal ions on the photochemical, photophysical, and antibacterial properties of three cationic porphyrin-triphenylphosphonium conjugates was investigated for the first time. Coordination with Zn(II), Pd(II) and Co(II) enabled fine-tuning of these conjugates properties, with Zn(II) complexes demonstrating particular promise. While Pd(II) and Co(II) complexes failed to generate singlet oxygen ($^1O_2$), thereby reducing their efficacy in bacteria photoinactivation, Zn(II) complexes exhibited efficient $^1O_2$ generation and strong bacterial adhesion. Among these, the Zn(II) metalloporphyrin **2-Zn**, featuring a well-optimized structure with three triphenylphosphonium units and six positive charges, showed exceptional effectiveness against Gram-negative *Escherichia coli* at lower concentrations. It significantly outperformed its free-base counterpart, reducing the required irradiation time by more than 65 %. Furthermore, **2-Zn** demonstrates to be safe, exhibiting no cytotoxicity towards Vero cells. These findings highlight the potential of Zn(II) porphyrin-triphenylphosphonium complexes as efficient photosensitizers for antimicrobial photodynamic therapy (aPDT), offering a promising approach to address the growing challenge of antibiotic bacterial resistance in both clinical and environmental contexts.

1. Introduction

The rise of severe and difficult-to-treat infections caused by multidrug-resistant bacterial strains is a direct consequence of the increasing prevalence of antimicrobial resistance, largely due to the widespread misuse of antibiotics [1–3]. These multidrug-resistant strains present a growing threat to public health, making it imperative to develop new antimicrobial therapies that are both rapid and effective, without further contributing to the development of resistant strains [4–9]. Recently, antimicrobial photodynamic therapy (aPDT) has emerged as a promising alternative to conventional treatments, enabling the rapid and efficient eradication of bacteria [5–7,10–17]. This therapy involves the use of a photosensitizer (PS) that, when activated by irradiation at a specific wavelength in the presence of molecular oxygen, generates highly cytotoxic Reactive Oxygen Species (ROS). These ROS oxidize various cellular components, leading to microbial inactivation [5,10,18–23].

Porphyrin derivatives are the most widely used class of PS in aPDT [24]. Their versatility enables chemical modifications to enhance solubility, target specificity, and photostability. Their highly conjugated structures enable effective light absorption in the visible region of the electromagnetic spectrum (400–700 nm). Upon being exposed to light, porphyrins transition to an excited singlet state, which can subsequently undergo by intersystem crossing process to a triplet state. Through type I and type II mechanisms, this process leads to the generation of ROS. Despite their advantages, porphyrins face some limitations in clinical applications, including weak absorption in the near-infrared region – where light penetration into tissues is deeper – and low solubility in biological aqueous environments [6,19,25–31]. To address these challenges, there has been a concerted effort to develop PS with improved biological properties. For tetrapyrrolic PS, their properties can be modified through structural fine-tuning by altering the substituents on the periphery of the macrocycle or by modifying the electronic environment at its core, often through metal coordination [29,32–38]. In porphyrin derivatives, the core cavity makes them exceptional ligands for forming complexes with a wide range of metal ions, resulting in the

* Corresponding authors.
E-mail addresses: aalmeida@ua.pt (A. Almeida), nmoura@ua.pt (N.M.M. Moura).

https://doi.org/10.1016/j.inoche.2025.114426
Received 29 January 2025; Received in revised form 25 March 2025; Accepted 26 March 2025
Available online 27 March 2025

formation of metalloporphyrins [39–41]. The coordination of a wide range of metal ions with tetrapyrrolic macrocycles has been widely demonstrated to be useful across various fields, including medicine, bioimaging, optoelectronics, photocatalysis, chemosensing, light-harvesting, and supramolecular chemistry [39,40,42–49]. In the context of antimicrobial photoinactivation, several studies have reported that metalloporphyrin derivatives exhibit enhanced photodynamic efficacy compared to their corresponding free base derivatives. This improvement is often attributed to their superior production of $^1O_2$ and/or improved cellular internalization of the PS [29,49,50].

Calmeiro and coworkers synthesized both free base and Zn(II) complexes of *meso*-tetraarylporphyrins functionalized with either methoxypyridinium or thiopyridinium groups [51]. The study revealed that only the Zn(II) complex with methoxypyridinium units effectively reduced the viability of *Escherichia coli* (*E. coli*), whereas the free base derivative of the thiopyridinium analog was more effective than the corresponding Zn(II) complex. However, the low photostability was highlighted as a significant drawback of these PS, which compromised their effectiveness in the photodynamic processes [51].

Galstyan *et al.* also investigated the efficacy of Zn(II) and Pd(II) complexes of π-extended porphyrins compared to the corresponding free base derivative in the photoinactivation of Gram-positive bacteria *Staphylococcus aureus* (*S. aureus*) and *Bacillus subtilis (B. subtilis)*. The results demonstrated that metal coordination into the porphyrin core enhanced the photodynamic activity of the PS, particularly Pd(II). This complex showed a significant increase in triplet state quantum yield for $^1O_2$ generation compared to the free-base porphyrin, thereby improving its photodynamic efficacy against the tested Gram-positive bacterial strains [29].

Recently, Dabrowski and colleagues reported similar findings after evaluating the antimicrobial photodynamic performance of Zn(II) and Pd(II) complexes of 2,6-difluorinated *meso*-tetraarylporphyrin derivatives against both Gram-negative and Gram-positive bacteria. The Pd(II) complex demonstrated a remarkable ability to generate $^1O_2$ making it an excellent PS capable of effectively reducing the viability of *S. aureus* biofilms. However, the uptake of both Zn(II) and Pd(II) metalloporphyrins was significantly reduced in *Pseudomonas aeruginosa* (*P. aeruginosa*) and *E. coli*, two Gram-negative bacterial strains. As a result, the ability to reduce the viability of these bacteria was compromised, particularly for *E. coli*, where the reduction was less than 1.5 Log CFU (below 97 % of bacterial reduction) [52].

Beyene and Wassie investigated the photosensitizing properties of a series of Cu(II) and Co(II) complexes of *meso*-tetraarylporphyrins bearing electron-donating and electron-withdrawing groups against Gram-positive and Gram-negative bacteria. The study revealed that Co(II) complexes with electron-withdrawing groups at the *para*-positions exhibited superior photodynamic performance compared to their Cu(II) counterparts. This enhanced antibacterial activity of Co(II) metalloporphyrins was attributed to their higher lipophilicity [53].

In a recent publication, we reported the remarkable antimicrobial photodynamic properties of cationic porphyrin-triphenylphosphonium derivatives **1**–**3** (Fig. 1) against the Gram-negative strain of *E. coli* and the Gram-positive methicillin-resistant *S. aureus* (MRSA) [54]. Compounds **1** and **2** exhibited outstanding efficacy against both bacterial strains, reducing bacterial viability to the detection limit of the method (>99.9999 %) with a significant reduction in irradiation time – 50 to 66 % less compared to the well-studied 5,10,15,20-tetrakis(1-methylpyridinium-4-yl)porphyrin (**TMPyP**), which was used as a reference. Moreover, these PSs were effective at concentrations of 1.0 μM or lower and demonstrated remarkable photostability and $^1O_2$ generation capability. The superior photodynamic activity of these compounds was attributed to these properties and the enhanced interaction with bacterial cells promoted by the presence of peripheral triphenylphosphonium groups.

Building on the promising results obtained with the free-base porphyrin derivatives bearing triphenylphosphonium units and the potential to enhance their photodynamic efficacy through metal coordination, we synthesized and characterized Zn(II), Pd(II) and Co(II) complexes of porphyrin **1**, and evaluated their photodynamic efficiency against Gram-negative and Gram-positive bacterial models. Based on these findings, the study was further extended to include Zn(II) complexes of porphyrins **2** and **3** (Fig. 1).

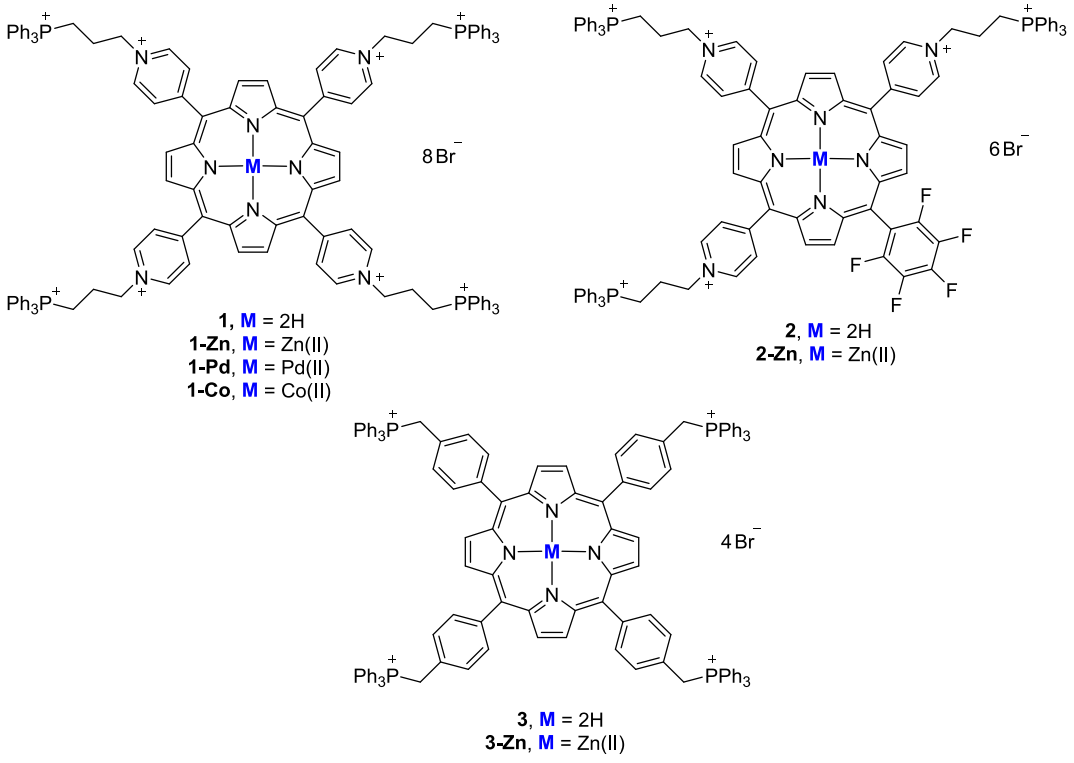

Fig. 1. Structures of the free-base and metallocomplexes porphyrin-triphenylphosphonium conjugates under study.

2. Results and discussion

2.1. Photosensitizers characterization

In selecting Zn(II), Pd(II), and Co(II) to prepare the new complexes **1-Zn**, **1-Pd**, and **1-Co**, as well as **2-Zn** and **3-Zn,** we considered literature reports highlighting the ability of these metal ions to improve the PS efficiency [29,51–53]. The complexes were synthesized using well-established methods [55–57], and metal ion insertion was readily confirmed through proton nuclear magnetic resonance (^{1}H NMR; Figs. S1–S5 in the ESI), FTIR (Figs. S6–S10, ESI) and UV–VIS spectroscopy.

To gain insight into the relationship between the biological activity of each complex with its photophysical properties, the absorption and emission properties of complexes were recorded in phosphate buffer solution (PBS) at 298 K (Table 1 and Fig. 2).

All metalloporphyrins exhibit a Soret band ascribed to π–π* transitions from the ground state to the second excited state ($S_0 \rightarrow S_2$), with an absorption maximum ranging from 430 to 440 nm. This represents a red-shift of 12 and 13 nm for complexes **1-Zn** and **2-Zn**, respectively, compared to the corresponding free base previously reported [54]. This bathochromic shift is likely due to the increased electron density of the porphyrin, which may be advantageous for clinical applications [58]. However, complex **3-Zn** did not show a noticeable bathochromic shift in the Soret band absorption maximum. The substitution of the hydrogen atoms in the core by metal ions induces a D_{4h} and C_{2h} geometry for metalloporphyrins **1**, **3** and **2**, respectively, and orbital degeneration resulting in the expected appearance of only one or two Q bands, attributed to the weak π–π* transitions from $S_0 \rightarrow S_1$ and higher molecular symmetry [58,59]. While the Zn(II) complexes display two Q bands with absorption maxima ranging from 563 to 609 nm, the Pd(II) and Co(II) complexes show only one Q band at 528 and 547 nm, respectively. The spectroscopic features observed for these two complexes (**1-Pd** and **1-Co**) are likely attributable to their lower solubility in PBS and a higher tendency to form aggregates as evidenced by the broadened Soret band. Regarding the emission spectra of the metalloporphyrins, it was observed that only the Zn(II) complexes **1-Zn** and **2-Zn** are emissive compounds, displaying an emission band with a maximum centered at 643 and 635 nm, respectively. The non-emissive behavior of the remaining derivatives (**1-Pd**, **1-Co** and **3-Zn**) in PBS can be attributed to a significant aggregation of the metalloporphyrins in this conditions, which restricts their intramolecular movements and promotes aggregates formation [60]. The data show that the absorption and emission profile of porphyrin-triphenylphosphonium complexes in PBS are less impacted in compounds with a higher number of positive charges and those metalated with Zn(II), mainly due to their improved solubility in PBS.

Knowing that the photodynamic performance of porphyrin-based PS can be significantly influenced by its stability, whether in the absence or presence of light, we examined the behavior of all porphyrin complexes in PBS. These assays were conducted by monitoring the Soret band maximum, both in the dark and under the same irradiation conditions used in the biological experiments, over 30 min. The results are summarized in Table 2.

Under dark conditions, the Zn(II)-based metalloporphyrins showed a moderate decrease in the Soret absorption, ranging from 15 % to 26 % after 30 min in solution. In contrast, the Pd(II) and Co(II) complexes of derivative **1** exhibited reductions of 35 % and 42 %, respectively. Under white light irradiation at an irradiance of 25 mW cm^{-2}, all metalloporphyrins showed a more significant reduction in the initial absorption at the Soret band maximum, with reductions ranging from 43 % for **3-Zn** to 51 % for **1-Zn** after 30 min of irradiation. In contrast to the free-base derivatives **1** and **2**, which displayed excellent (photo)stability [54], the introduction of metal ions into the porphyrin-triphenylphosphonium core led to a much more pronounced decrease in the Soret band absorption. This may be due to increased aggregation and the formation of molecular clusters in the Pd(II) and Co(II) complexes, as indicated by the pronounced reductions observed under dark conditions. These findings, combined with the low molar absorption coefficient, suggest lower solubility in aqueous media. For the Zn(II) complexes, light appears to induce some photodegradation, particularly in derivatives **1-Zn** and **2-Zn**, where the reduction values did not exceed 32 %, considering the reduction due to aggregation phenomena during the experiment.

Considering that the production of ROS, namely singlet oxygen ($^1O_2$) by a PS is closely related to its photodynamic efficiency, this property was also evaluated for all complexes in DMF. These assays were performed using an indirect method based on the photo-oxidation of 1,3-diphenylisobenzofuran (DPiBF), a $^1O_2$ scavenger with a maximum absorption at 415 nm. When it reacts with $^1O_2$ in a [4 + 2] cycloaddition process, it forms the colorless compound 1,2-dibenzoylbenzene [61–63]. The results obtained are summarized in Fig. 3 along with the data for the free-bases **1**–**3** for comparison. Apart from **1-Co** complex, all the PS were able to generate appreciable amounts of $^1O_2$ in DMF solutions. Although, in general the introduction of metal ions reduced $^1O_2$ production compared to the corresponding free-base counterparts, **3-Zn** surpasses the $^1O_2$ production of its free-base**.** This complex exhibited a 2-fold higher capability to generate $^1O_2$ compared to the free-base counterpart **3** and 25 % more than the free-base **1** and **2**, which were already recognized as good $^1O_2$ generators [64]. The higher $^1O_2$ production exhibited by this Zn(II) complex **3-Zn** is likely due to its ability to accelerate the transitions between excited electronic states, enhancing the population of the triplet excited state, which is crucial for producing $^1O_2$ [59].

Both complexes **1-Zn** and **2-Zn** demonstrated a similar ability to generate $^1O_2$, though their efficiency was about 2.5 times lower compared to their free-base derivatives. It was also noted that the incorporation of Pd(II) into the porphyrin core significantly reduced the ability of the porphyrin-triphenylphosphonium complex **1-Pd** to generate this ROS species. Its efficiency dropped by around 80 % compared to the free-base PS **1** and 50 % compared to the Zn(II) complex **1-Zn**.

It is important to point out that under similar irradiation conditions there was no noticeable decrease in DPiBF absorption in the control sample, which did not contain PS. This data clearly shows that most of the complexes play a key role in generating $^1O_2$, the reactive oxygen species responsible for scavenger decomposition.

Table 1
Photophysical properties of the metalloporphyrins evaluated in PBS at 298 K.

Compd	Soret band (nm)	log ε	Q bands (nm)	log ε	λ $_{em}$ (nm)
1-Zn	440	5.06	564	4.02	643
			609	3.76	
1-Pd	430	4.60	528	4.21	–[a]
1-Co	439	4.47	547	3.69	–[a]
2-Zn	436	5.11	562	4.10	635
			603	3.68	
3-Zn	430	4.89	562	3.81	–[a]
			602	3.65	

[a] Non-emissive compound.

2.2. aPDT efficacy of metalloporphyrins

Although some complexes showed photophysical and photochemical features that could affect their aPDT effectiveness, all of them were subjected to assays to compare their photodynamic efficiency. These studies were conducted against MRSA and *E. coli* as Gram-positive and Gram-negative bacteria models, respectively. The results were compared with the values obtained previously for free base porphyrins **1**–**3** [54] which were used as reference. These studies were complemented by bacterial uptake assessment and cytotoxicity assays with the most promising PS in Vero cells.

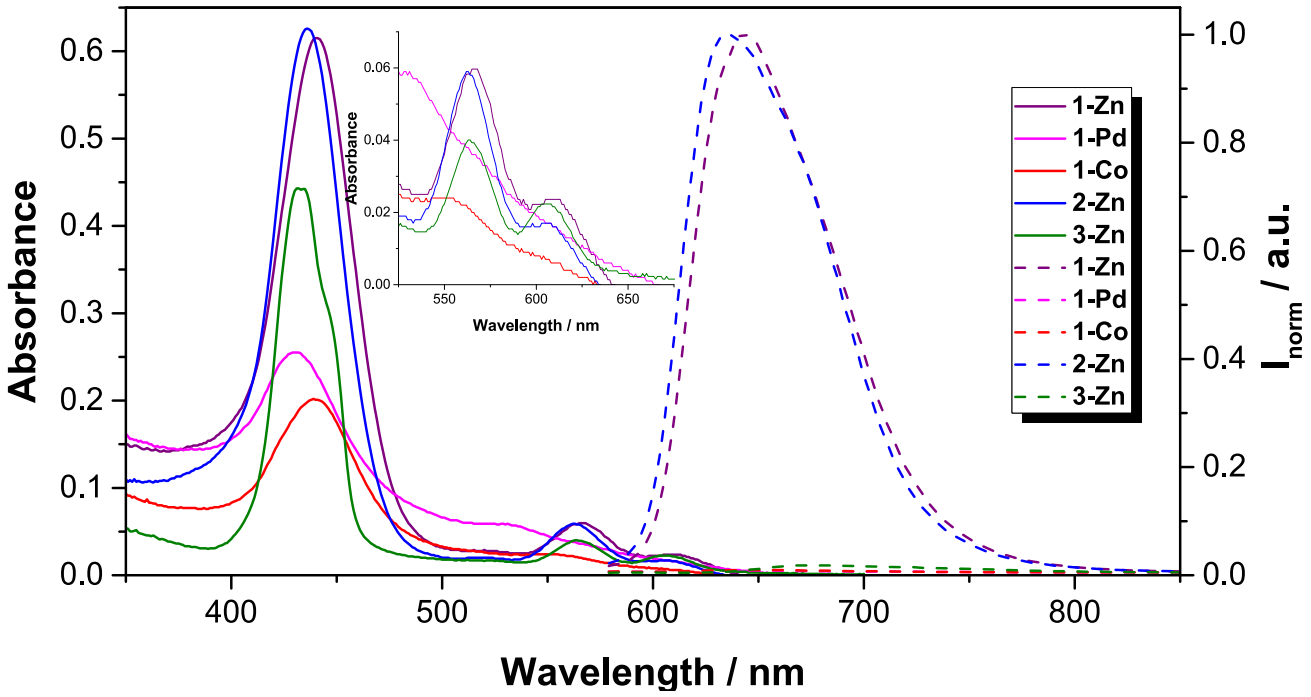

Fig. 2. Absorption (solid line) and normalized emission (dash line) spectra of porphyrin-triphenylphosphonium conjugates complexes **1Zn**, **1-Pd**, **1-Co**, **2-Zn** and **3-Zn** in PBS at 298 K ($\lambda_{exc1\text{-}Zn}$ = 440 nm; $\lambda_{exc1\text{-}Pd}$ = 430 nm; $\lambda_{exc1\text{-}Co}$ = 439 nm; $\lambda_{exc2\text{-}Zn}$ = 436 = 423 nm; $\lambda_{exc3\text{-}Zn}$ = 430 nm). The inset shows the absorption at Q bands region.

Table 2
Percentage of Soret band reduction for metalloporphyrins assessed at a concentration of 5.0 μM after exposure to dark conditions or irradiation with white light at an irradiance of 25 mW cm^{-2} in pre-established intervals (0–30 min).

Conditions	PS	λ_{max} (nm)	Experimental Time (min)*				
			0	5	10	15	30
Dark	1-Zn	440	0	10	15	20	22
	1-Pd	430	0	14	24	29	35
	1-Co	439	0	29	34	39	42
	2-Zn	436	0	4	7	11	15
	3-Zn	432	0	5	6	14	26
Light	1-Zn	440	0	21	27	35	51
	1-Pd	430	0	4	10	18	43
	1-Co	439	0	5	21	23	47
	2-Zn	436	0	11	36	37	47
	3-Zn	432	0	15	26	34	45

* The results are expressed as the percentage of absorption decay, calculated by the ratio of absorbance at λ_{max} at different time intervals to the absorbance before irradiation (t = 0 min).

2.3. Bacterial adhesion

The adherence features of PS to bacterial cells are a key factor in aPDT, as strong adherence enhances the potential for ROS production at the target site. The ability of each metalloporphyrin to attach to bacterial structures was evaluated. The tests were carried out on both Gram-positive (MRSA) and Gram-negative (*E. coli*) bacterial models, using the highest concentrations tested in the biological experiments: 0.5 μM and 5.0 μM, respectively. The results are shown in Fig. 4.

The data showed that apart of complex **1-Pd**, the complexes **1-Zn and 1-Co** exhibited higher adsorption levels to both methicillin-resistant *S. aureus* and *E. coli* bacterial cells compared to the free-base PS **1** ($p < 0.05$, ANOVA). These results are consistent with our previous study, where we demonstrated that the presence of triphenylphosphonium moieties on porphyrin periphery significantly enhances cellular adhesion compared to the reference **TMPyP** [54].

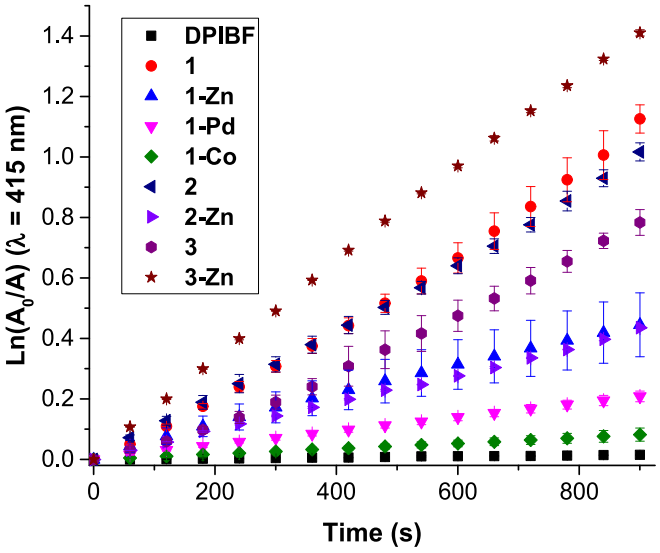

Fig. 3. Evaluation of the decomposition of DFiBF (50 μM) in the presence or absence of the metalloporphyrins **1-Zn**, **1-Pd**, **1-Co**, **2-Zn** and **3-Zn** and of the corresponding free-bases **1–3** at a concentration of 0.5 μM in DMF, under irradiation with red light (630 nm ± 20 nm) at an irradiance of 15 mW cm^{-2}.

Additionally, the Zn(II) complexes **1-Zn**, **2-Zn** and **3-Zn** showed a higher affinity for bacterial cells than the other PS, with values of 2.9 × 10^4, 2.6 × 10^4 and 1.8 × 10^5 PS Molecules/CFU mL^{-1} for *S. aureus*, and 4.2 × 10^4, 4.8 × 10^4 and 9.5 × 10^5 PS Molecules/CFU mL^{-1} for *E. coli*, respectively ($p < 0.05$). This suggests that incorporating Co(II) and Zn (II) atoms at the porphyrin core improves the adhesion of PS to bacterial surfaces. In particular, the impressive results obtained with the Zn(II) complexes can be attributed to their strong capacity to binding phosphate groups, particularly the anionic phospholipids on the bacterial cell

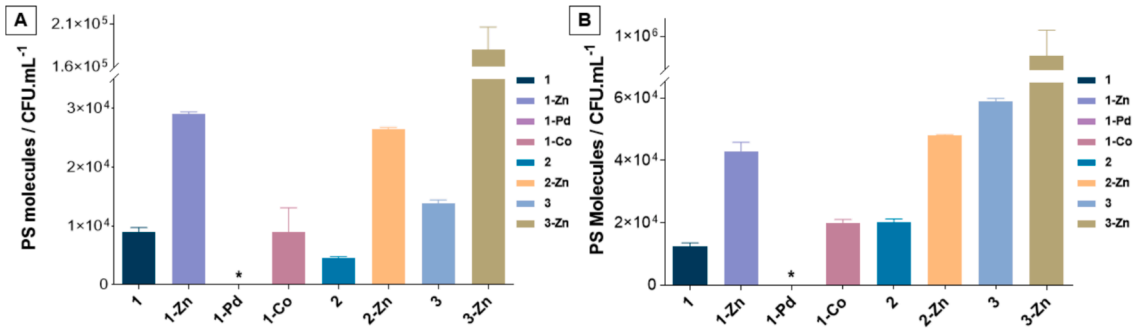

Fig. 4. The cellular adhesion of porphyrin-triphenylphosphonium derivatives **1**–**3** and their corresponding metalloporphyrin complexes to methicillin-resistant *S. aureus* (A) and *E. coli* (B) assessed at the concentrations of 1.0 and 5.0 μM, respectively. The data shown represent the mean of two independent experiments, each performed in duplicate. Error bars indicate standard deviation (SD), and * indicates cases where there is no fluorescence, impossible to quantify.

membrane [65,66]. However, the apparently higher adhesion of **3-Zn** (1.8×10^5 and 9.5×10^5 PS Molecules/CFU mL^{-1} for *S. aureus* and *E. coli*, respectively) in both bacterial strains is certainly related to its poor solubility in aqueous media, leading to the formation of PS aggregates on the bacterial cell surface which dramatically affect the uptake values of this complex.

2.4. aPDT efficacy against methicillin-resistant S. aureus

The effectiveness of each metalloporphyrins (**1-Zn**, **1-Pd**, **1-Co, 2-Zn** and **3-Zn**) in the photoinactivation of methicillin-resistant *S. aureus*, a Gram-positive bacterial model, was assessed over 90 min using white light (380–700 nm) at an irradiance of 25 mW cm^{-2}. The assays were conducted with each PS at a concentration of 0.5 μM and using the adequate free-base porphyrin-triphenylphosphonium conjugates **1**–**3** for comparison. It is worth noting that in our previous study we found that derivatives **1** and **2** surpassed the photodynamic activity of **TMPyP**, commonly used as a reference, with an irradiation time reduction of more than 65 %. PS **3** exhibited a photoinactivation profile similar to that of **TMPyP** against MRSA [54].

The first assays were performed with all the complexes of conjugate **1** in order to evaluate the impact of different metal ions, Zn(II), Pd(II) and Co(II), on their photodynamic efficiency. The results shown in Fig. 5 indicate that only the **1-Zn** demonstrated promising photoinactivation results, having driven to bacterial reduction to the detection limit of the method used to quantify the bacteria (~7.2 log CFU mL^{-1}, $p < 0.05$) after 30 min of photodynamic treatment (Fig. 5A). The octacationic metalloporphyrins **1-Pd** and **1-Co** did not promote any reduction in the viability of methicillin-resistant *S. aureus* (Fig. 5B,C). Nevertheless, the free-base porphyrin **1** proved to be more effective than **1-Zn**, considering that the same effect was achieved in a shorter photodynamic treatment (15 min).

Acknowledging that only the Zn(II) complex **1-Zn** demonstrated promising biological activity conducting to the total bacterial reduction, contrary to the Pd(II) and Co(II) complexes, we decided to assess the corresponding Zn(II) metalloporphyrins of derivatives **2** and **3**. The results from photodynamic inactivation assays against MRSA in the presence of both complexes **2-Zn** and **3-Zn** are summarized in Fig. 6.

Complex **3-Zn** was able to induce a reduction in the viability of MRSA at a concentration of 0.5 μM (Fig. 6B). However, the photodynamic effect of **3-Zn** achieved only a reduction of approximately 4.8 CFU mL^{-1} (>99.99 %) after 45 min of irradiation ($p < 0.05$, ANOVA).

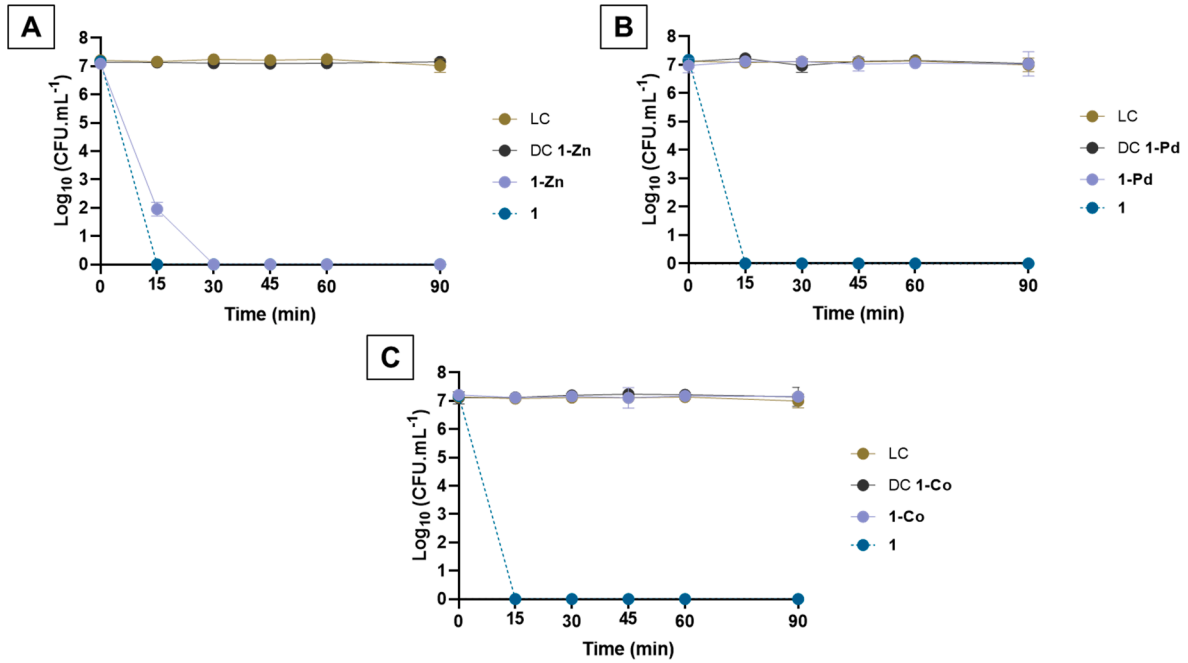

Fig. 5. Photodynamic inactivation profile of methicillin-resistant *S. aureus* induced by metalloporphyrin-based PS **1-Zn** (A), **1-Pd** (B) and **1-Co** (C) at a concentration of 0.5 μM, irradiated with white light at an irradiance of 25 mW cm^{-2}, compared to PS **1**. LC – light control; DC – dark control. Values are presented as the mean of 3 independent assays, each with two replicates; standard deviations are represented by error bars. Lines are used to connect experimental data points.

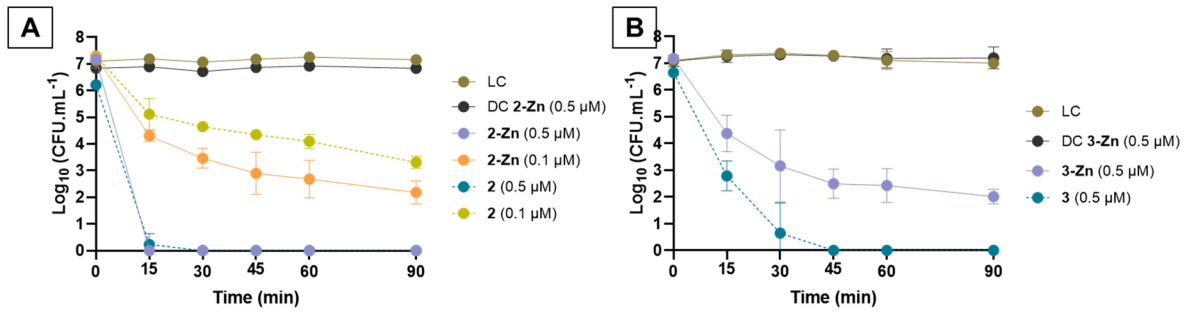

Fig. 6. Photodynamic inactivation profile of methicillin-resistant *S. aureus* induced by metalloporphyrin-based PS **2-Zn** at 0.5 and 0.1 μM (A) and **3-Zn** at 0.5 μM (B) irradiated with white light at an irradiance of 25 mW cm^{-2}, compared to PS **2** and **3**, respectively. LC – light control; DC – dark control. Values are presented as the mean of 3 independent assays, each with two replicates; standard deviations are represented by error bars. Lines are used to connect experimental data points.

Extending the photodynamic treatment did not result in any significant improvement in bacterial photoinactivation ($p < 0.05$, ANOVA). For compound **3-Zn**, the presence of zinc(II) in the porphyrin core did not enhance its photodynamic performance and resulted in a significant reduction in photodynamic efficacy compared to the one obtained with the free-base **3**. In that case, at the same concentration, only one-third of the treatment time (15 min) was required to achieve the same reduction in bacterial viability, with complete photoinactivation (>99.99999 %) of *S. aureus* reached after 45 min of treatment.

The results presented in Fig. 6A for complex **2-Zn** were much more promising. The positive impact of the Zn(II) ion was evident at a concentration of 0.5 μM, with the metalloporphyrin **2-Zn** leading to bacterial reduction until the detection limit of the method [~7.2 log CFU mL^{-1}] after 15 min of irradiation ($p < 0.05$, ANOVA). This level of photodynamic efficiency in decreasing MRSA viability was comparable to that observed with the corresponding free-base porphyrin-triphenylphosphonium **2**. Given the impressive performance of **2-Zn**, we decided to lower the PS concentration to 0.1 μM and assess its photodynamic profile.

At the reduced concentration (0.1 μM), **2-Zn** showed a ~5.0 log CFU mL^{-1} (~99.999 %) reduction in *S. aureus* viability after 90 min of irradiation ($p < 0.05$). This reduction in bacterial viability represents a significant enhancement in the photodynamic efficacy, compared to the free-base derivative **2**, which under the same conditions resulted in a reduction of only 3.9 log CFU mL^{-1} (99.99 %) (Fig. 6A).

2.5. aPDT efficacy against E. coli

The photodynamic efficacy of the metalloporphyrins was assessed using a bioluminescent strain of *E. coli* as a Gram-negative model. This strain serves as an excellent model for monitoring photodynamic efficacy, as its light emission is a sensitive indicator of metabolic activity [67]. Furthermore, the bioluminescent approach enables real-time detection of microbial viability, offering a faster and more cost-effective alternative to conventional plating methods.

Considering the lower susceptibility of *E. coli* to aPDT approach compared to Gram-positive bacteria, the metalloporphyrins were tested at the concentrations of either 5.0 or 1.0 μM, based on their effectiveness (Fig. 7). The photodynamic activity was assessed over 90 min of white light irradiation (380–700 nm) at an irradiance of 25 mW cm^{-2}.

The results showed that similarly to the photodynamic inactivation assays for MRSA, the complexes **1-Pd** and **1-Co** did not show any significant reduction in Gram-negative bacteria viability at a concentration of 5.0 μM and after 90 min of treatment ($p > 0.05$) (data not showed). In

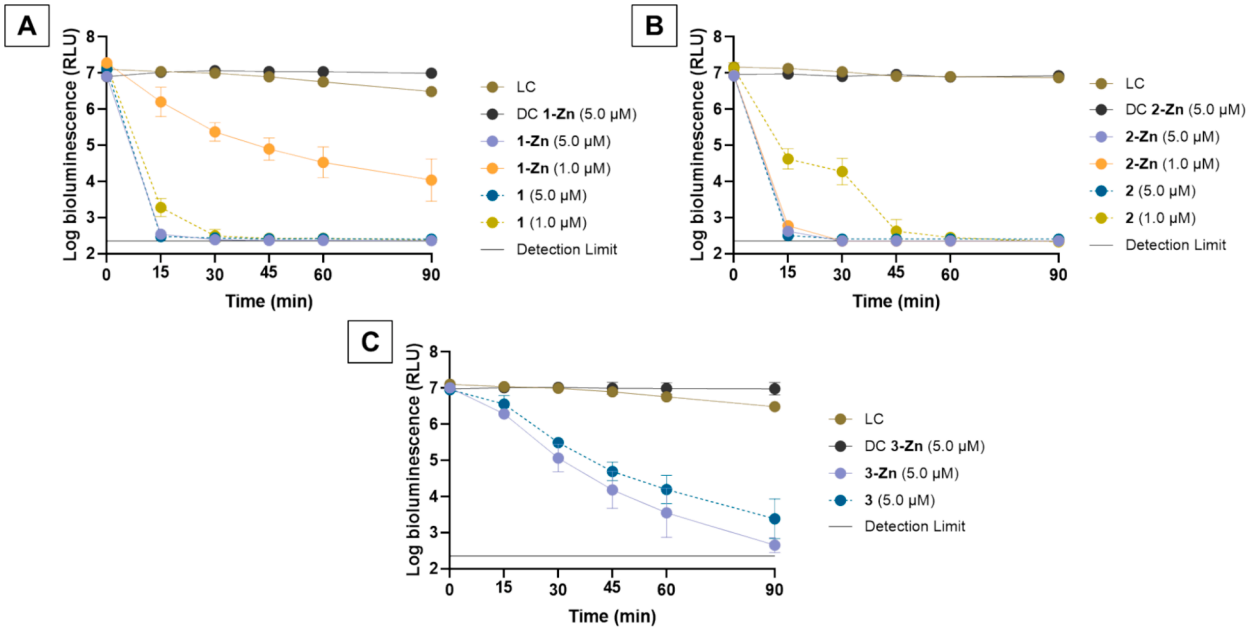

Fig. 7. Photodynamic inactivation profile of bioluminescent *E. coli* induced by metalloporphyrin-based PS **1-Zn** (A) and **2-Zn** (B) both at 5.0 and 1.0 μM, and **3-Zn** (C) at 5.0 μM, irradiated with white light at an irradiance of 25 mW cm^{-2}, compared to the adequate free base porphyrin-triphenylphosphonium PS **1**–**3**. LC – light control; DC – dark control. Values are presented as the mean of 3 independent assays, each with two replicates; standard deviations are represented by error bars. Lines are used to connect experimental data points.

contrast, metalloporphyrin **1-Zn**, at a concentration of 5.0 μM retains the excellent photodynamic efficiency of the free-base porphyrin-triphenylphosphonium **1**, reaching the detection limit of the method after just 15 min of treatment, leading to a reduction in bacterial bioluminescence by ~4.6 log RLU (Fig. 7A). However, at the lower tested concentration (1.0 μM), metalloporphyrin **1-Zn** achieved a maximum reduction of ~2.5 log RLU after 90 min of treatment ($p < 0.05$), while the free-base **1** was able to reduce the *E. coli* bioluminescence signal (~4.6 log RLU) to the detection limit of the method after 30 min of irradiation.

The results for metalloporphyrins **2-Zn** and **3-Zn**, shown in Fig. 7 (B and C), reveal that the incorporation of the Zn(II) ion in the free-base derivatives **2** and **3** had a beneficial effect, significantly enhancing the photodynamic activity of both porphyrins ($p < 0.05$) against *E. coli*. At a concentration of 5.0 μM, the metalloporphyrin **2-Zn** promoted a rapid and pronounced decrease in the bacterial bioluminescence signal, reaching the detection limit of the luminometer, with a reduction of ~4.7 log RLU ($p < 0.05$) after 15 min of treatment, comparable to the results achieved with the free base conjugate **2**. However, when the PS concentration was reduced to 1.0 μM, the PS **2-Zn** demonstrated a notable enhancement in the photoinactivation profile compared to the free-base porphyrin-triphenylphosphonium **2**, which needed 45 min of treatment to produce the same level of photoinactivation. At 1.0 μM, **2-Zn** achieved the same efficacy as at 5.0 μM, resulting in a reduction of the *E. coli* bioluminescence to the detection limit of the method after just the same 15 min of treatment (Fig. 7B).

The metalloporphyrin **3-Zn** at a concentration of 5.0 μM achieved a reduction of ~4.1 log RLU ($p < 0.05$) in the bacterial bioluminescence signal after 90 min of treatment, nearing the detection limit of the luminometer. In comparison, the corresponding free base PS **3** produced only a ~3.1 log RLU reduction in the bioluminescence signal at the same concentration (Fig. 7C).

Across all experiments, no significant changes in viable MRSA cell concentrations and *E. coli* bioluminescence signal ($p > 0.05$) were observed in either the light or dark controls (LC and DC) for any of the tested compounds during the treatment period. This indicates that the experimental conditions did not impact the bacterial viability, nor did the PS induce cytotoxicity in the dark at the tested concentrations.

Overall, the assessment of the photodynamic activity of the selected metalloporphyrins containing triphenylphosphonium groups demonstrated that Zn(II)-coordinated metalloporphyrins do not compromise their ability to act as PS in aPDT, and can even have a beneficial effect. Despite exhibiting higher aggregation, slightly reduced (photo)stability and in general lower efficiency to generate $^1O_2$ compared to the free-base counterparts, the Zn(II) complexes still exhibited notable photodynamic activity towards both bacterial strains.

It is important to note that despite the improved $^1O_2$ generation observed in **3-Zn** this PS did not achieve complete photoinactivation of either bacterial model after 90 min of treatment. This may be attributed to its strong tendency to form aggregates in aqueous solutions, demonstrated by the artificial adhesion observed, which can quench $^1O_2$ generation and, consequently, leading to diminished PS activity against MRSA and *E. coli*. Previous studies have shown that, while cell affinity is crucial for effective bacterial photoinactivation, a high level of adhesion does not always correlate into enhanced antimicrobial effects against both Gram-positive and Gram-negative bacteria [68,69]. In this context, other factors, such as structural features, the number and localization of positive charges, and the ability to generate $^1O_2$, might play a more critical role in influencing photodynamic activity [68,70].

Despite its aggregation behavior and slightly reduced (photo)stability compared to its free-base counterparts, the Zn(II) complex **2-Zn** exhibited remarkable photodynamic activity against both MRSA and *E. coli*. Remarkably, the efficiency of **2-Zn** surpassed that of the other Zn (II) complexes and free-base derivatives against *E. coli*, particularly at lower concentrations where aggregation is less pronounced. This led to a significant reduction in irradiation time from 45 to 15 min, compared to the free-base **2**. This enhanced performance is probably due to a well-balanced combination of the number of positive charges, the presence of triphenylphosphonium units, the electron-withdrawing pentafluorophenyl group, and better cellular adhesion, which together provide the conjugate with more favorable properties as a PS.

2.6. Cytotoxicity assays in Vero cells

For the clinical application of aPDT, it is crucial to ensure both the effectiveness of the PS and the absence of toxicity to host cells. In our previous study using the free-base porphyrin-triphenylphosphonium conjugates **1**–**3**, potential toxicity was observed during photodynamic inactivation assays on *S. aureus* in the incubation period. This effect was only notable for porphyrin **2** at a concentration of 0.5 μM, resulting in a reduction in bacterial count (1.4 log CFU mL^{-1}, $p < 0.05$). While this may be linked to the bactericidal properties of the triphenylphosphonium groups, it remains important to ensure that such toxicity does not affect surrounding tissues [71].

Based on these findings and the possible clinical applications of these new PS, cytotoxicity tests were performed to assess their safety. The viability of Vero cells was measured, following treatment with the most effective PS, using the Resazurin assay (see details in the experimental part). The assays were performed in the presence of Zn(II) complexes, **1-Zn**, **2-Zn**, and **3-Zn**, and their porphyrin-triphenylphosphonium conjugates **1–3**, and compared to untreated control cells. The assays were performed at three concentrations: 0.5, 1.0, and 5.0 μM (Fig. 8).

These assays allowed to conclude that none of the evaluated conjugates demonstrated cytotoxicity towards Vero cells at any of the three tested concentrations, including at 5.0 μM the highest concentration used in the biological assays ($p > 0.05$) (Fig. 8). These results confirm that both the free-base conjugates and their corresponding Zn(II) porphyrin-triphenylphosphonium PS exhibit no cytotoxicity in host cells and are safe at the tested concentrations. This safety combined with their high photosensitizing efficiency against bacteria, suggests that these derivatives could be suitable for future clinical applications.

3. Materials and methods

3.1. Synthesis of metalloporphyrins

Free-base porphyrin scaffolds were prepared as reported in a previous work [72]. Then the appropriate free-base porphyrin derivative was reacted with metal salts $Zn(OAc)_2$, $Pd(OAc)_2$ or $CoCl_2$ in methanol following a well-stablished procedure [55,73] to obtain the expected metalloporphyrins (**1-Zn**, **1-Pd**, **1-Co**, **2-Zn** and **3-Zn**) in yields ranging from 95 to 98 %.

1-Zn

Yield: 97 %. ^{1}H NMR (300 MHz, DMSO-d_6): δ 9.61 (8H, d, $J = 6.9$ Hz, H-*o*-Py), 9.09 (8H, s, H-β), 8.91 (8H, d, $J = 6.9$ Hz, H-*m*-Py), 8.02–7.89 (24H, m, H-*o*-PPh_3), 7.87–7.77 (36H, m, H-*m,p*-PPh_3), 5.32–5.12 (8H, m, CH_2), 4.21–4.00 (8H, m, CH_2), 3.68–3.30 (8H, m, CH_2 – overlapped with DMSO residual peak) ppm. FTIR (KBr) ν_{max}: 3428.70, 3055.29, 2923.36, 1594.05, 1439.09, 1407.35, 1338.89, 1111.12, 1047.64, 1015.28, 988.52, 883.34, 742.69, 682.95, 615.12, 532.97, 505.38 cm^{-1}.

1-Pd

Yield: 95 %. ^{1}H NMR (300 MHz, DMSO-d_6): δ 10.06–9.50 (8H, m, H-*o*-Py), 9.28–8.77 (16H, m, H-β and H-*m*-Py), 7.98–7.79 (60H, m, H-PPh_3), 5.28–4.98 (8H, m, CH_2), 3.96–3.77 (8H, m, CH_2), 2.69–2.58 (8H, m, CH_2 – overlapped with DMSO residual peak) ppm. FTIR (KBr) ν_{max}: 3433.05, 3055.09, 2927.31, 1637.10, 1431.41, 1349.76, 1180.85, 1098.57, 1016.30, 788.80, 688.45, 510.19 cm^{-1}.

1-Co

Yield: 98 %. ^{1}H NMR (300 MHz, DMSO-d_6): δ 10.07–9.52 (8H, m, H-*o*-Py), 9.36–8.74 (16H, m, H-β and H-*m*-Py), 7.97–7.75 (60H, m, H-

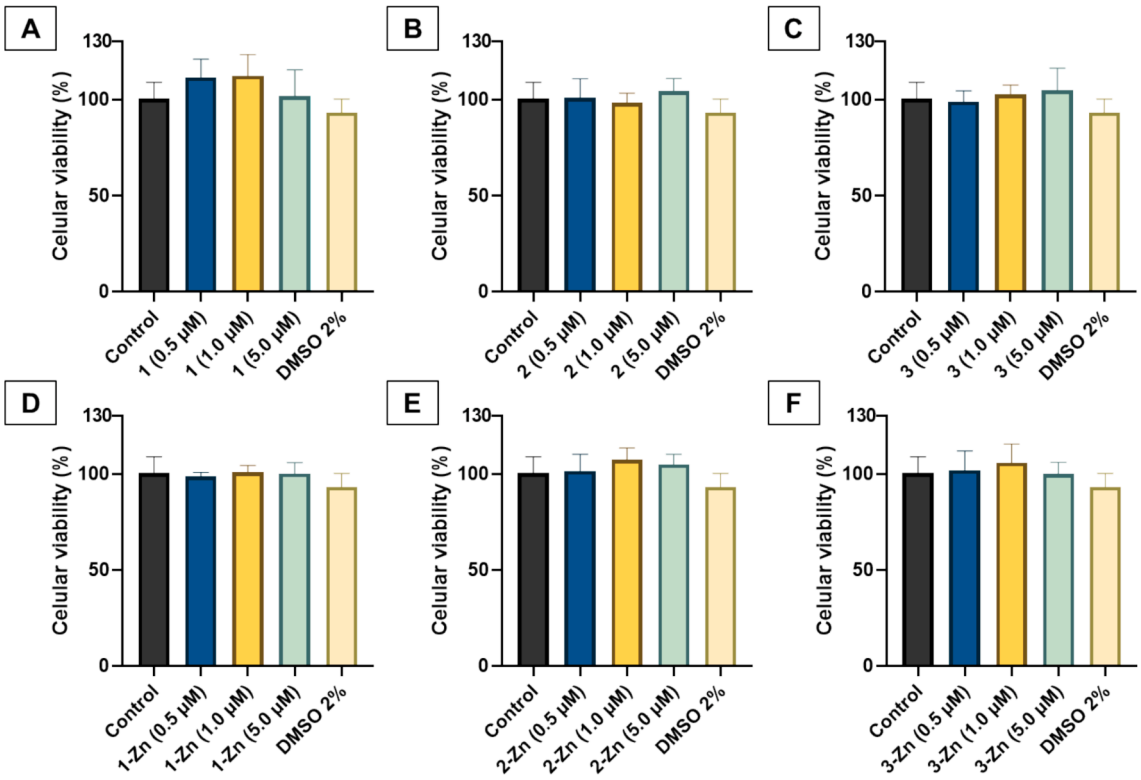

Fig. 8. Effect of PS **1** (A), **2** (B), **3** (C), **1-Zn** (D), **2-Zn** (E) and **3-Zn** (F), and 2 % DMSO solution on the viability of Vero cells. All PS were evaluated at three concentrations: 0.5, 1.0, and 5.0 μM. Cytotoxicity was determined after 24 h of exposure and compared to control cells (Control). Results are presented as the mean ± standard deviation from three independent experiments, each performed in triplicate, and are compared with the reduction of resazurin (%) observed in untreated control cells.

PPh_3), 5.24–4.99 (8H, m, CH_2), 3.94–3.76 (8H, m, CH_2), 2.66–2.59 (8H, m, CH_2 – overlapped with DMSO residual peak) ppm. FTIR (KBr) ν_{max}: 3428.70, 3046.58, 2923.36, 1630.14, 1548.00, 1434.73, 1352.58, 1175.22, 1111.12, 988.52, 796.84, 724.02, 687.93, 258.61, 491.89 cm^{-1}.

2-Zn

Yield: 97 %. ^{1}H NMR (300 MHz, DMSO-d_6): δ 9.63–9.48 (8H, m, H-*o*-Py), 9.27 (2H, d, J = 15.54 Hz, H-β), 9.16–9.03 (6H, m, H-β), 9.01–8.91 (6H, m, H-*m*-Py), 8.06–7.81 (45H, m, H-PPh_3), 5.28–5.08 (8H, m, CH_2), 4.14–3.95 (8H, m, CH_2), 2.71–2.60 (8H, m, CH_2 – overlapped with DMSO residual peak) ppm. FTIR (KBr) ν_{max}: 3415.00, 3050.94, 2919.00, 1584.71, 1434.73, 1398.01, 1334.54, 1190.20, 1106.76, 1048.71, 1021.29, 884.16, 738.31, 682.95, 606.17, 523.63, 505.58, 501.46 cm^{-1}.

3-Zn

Yield: 98 %. ^{1}H NMR (300 MHz, DMSO-d_6): δ 8.69 (8H, s, H-β), 8.14–7.78 (68H, m, H-*o*-Ph and H-PPh_3), 7.43–7.34 (70H, m, H-*m*-Ph), 5.53 (8H, d, J = 15.54 Hz, CH_2) ppm. FTIR (KBr) ν_{max}: 3419.36, 3055.29, 2932.69, 1566.67, 1429.75, 1338.89, 1201.98, 1106.76, 992.87, 796.84, 755.76, 724.02, 687.93, 605.78, 509.94, 478.20 cm^{-1}.

3.2. Absorption and emission spectra

UV–Vis absorption spectra were recorded in a UV-2501PC Shimadzu spectrophotometer from a 5.0 μM PBS solution of each metalloporphyrin, while emission spectra were recorded in a FluoroMax Plus spectrofluorometer from Horiba. Excitation was performed at the maximum of the Soret band for each compound, with a 5 nm slit width at an OD below 0.05.

3.3. Dark and photostability

A 2.5 mL solution of the adequate metalloporphyrin PS (5.0 μM) in PBS was prepared in a glass cuvette. For the dark stability assays, the solutions were gently stirred and kept in the dark. For the photostability assays, the solutions were exposed to a 30 W white light PAR LED system (LUMECO) with an irradiance of 25 mW cm^{-2}. The decrease in the Soret band absorption maximum for each PS was tracked at specific time intervals (0, 5, 10, 15, and 30 min) over a total period of 30 min, and the data were recorded using a HALO DB-20 Dynamica spectrophotometer.

3.4. Singlet oxygen generation

A 2.5 mL solution of DPiBF (50 μM) in DMF, along with each metalloporphyrin-based photosensitizer (0.5 μM) or free base derivatives **1**–**3** (0.5 μM), used as references, was prepared in a glass cuvette. The solutions were exposed to irradiation with a red-light LED array (λ = 630 ± 20 nm), while being gently stirred. The absorbance decrease of DPiBF was measured at its peak absorption wavelength (415 nm) at 60 s intervals over a period of 900 s.

3.5. Biological evaluation studies

3.5.1. Bacterial strains and growth conditions

The methicillin-resistant *S. aureus* strain DSM 25693 (MRSA), which produces staphylococcal enterotoxins A, C, H, G, and I, obtained from the Leibniz Institute DSMZ-German Collection of Microorganisms and Cell Cultures, was selected as the Gram-positive model [74]. The strain was stored on Tryptic Soy Agar (TSA) at 4 °C. For each experiment, three bacterial colonies were transferred to 25 mL of Tryptic Soy Broth (TSB) and incubated at 37 °C for 18–24 h at 120 rpm. Afterward, 250 μL of this culture were added to 25 mL of fresh TSB and incubated under the same

conditions to grow the bacteria to the stationary phase, reaching a concentration of ~10^9 CFU mL^{-1}.

The *E. coli* strain used in this study was genetically engineered in our laboratory by introducing two plasmids, pHK724 and pHK555, into chemically competent *E. coli* Top 10 cells. These plasmids carry the *lux* operon, which encodes the genes necessary for producing luciferase and other enzymes involved in light emission, derived from the naturally bioluminescent bacterium *Aliivibrio fischeri* [75]. Before each experiment, a bacterial suspension stored at −80 °C in 10 % glycerol was transferred into 25 mL of TSB and incubated at 25 °C for 18–24 h with continuous shaking at 120 rpm until the culture reached the stationary phase, corresponding to ~10^9 CFU mL^{-1}. The relationship between CFU mL^{-1} and the bioluminescence emitted by this strain has been previously established and documented [75].

3.5.2. PS cellular adhesion

Bacterial suspensions were prepared in PBS with a final concentration of ~10^7 CFU mL^{-1}, and the selected PS were added to reach a total volume of 2 mL. The suspensions were incubated for 15 min in the dark with gentle magnetic stirring at room temperature to promote PS interaction with the bacterial cells. The experiments were conducted at the maximum PS concentrations used in the photodynamic inactivation studies (1.0 μM for *S. aureus* and 5.0 μM for *E. coli*). Following the dark incubation, 1 mL of each sample and control was centrifuged for 5 min at 10,000 rpm. The supernatant containing unbound PS was discarded, and the bacterial pellet was washed three times with PBS, with centrifugation after each wash. The resulting pellets were resuspended in 500 μL of DMSO, then vortexed vigorously, sonicated for 30 min, and vortexed again to ensure bacterial cell disruption. The samples were transferred to dark 96-well microplates, and the fluorescence of PS bound to the cells was analyzed using a FluoroMax Plus spectrofluorometer with a 2 nm slit width. The excitation wavelength was set at 429 nm, and emission spectra were collected between 550 and 850 nm. Fluorescence intensity was used to quantify the PS concentration bound to the cells through comparison with a calibration curve constructed from known PS concentrations. Simultaneously, 1 mL aliquots of both the samples and controls were taken post-incubation to assess viable cell concentrations using the drop-seeding technique [76]. These aliquots were serially diluted in PBS, and 10 μL of each dilution was plated onto TSA plates, followed by incubation at 37 °C for 24 h. After incubation, colony counts from the appropriate dilution were used to calculate CFU mL^{-1}. All analyses were performed in duplicate, with two replicates for each assay (n = 4). The results were expressed as PS molecules per Log CFU mL^{-1}.

3.5.3. Antimicrobial photodynamic therapy assays

For each assay, bacterial suspensions in the exponential growth phase were diluted 1:100 in PBS and distributed into 6-well plates. The required volumes of each PS were added to achieve the desired final concentrations: 0.1 and 0.5 μM for methicillin-resistant *S. aureus*, and 1.0 and 5.0 μM for *E. coli*. These concentrations were chosen based on the known higher resistance of Gram-negative bacteria to aPDT compared to Gram-positive strains [70,76]. Control groups were also included, with light controls (LC) consisting of bacterial suspensions in PBS exposed to light, and dark controls (DC) consisting of bacterial suspensions treated with the PS but kept in the dark throughout the experiment. All controls and samples were incubated in the dark for 15 min with gentle agitation (120 rpm) to allow for PS binding to the bacterial cells. Following incubation, the LC and samples groups were irradiated with white light at an irradiance of 25 mW cm^{-2} for 90 min, while the DC groups remained shielded from light. Bacterial viability was assessed by collecting 150 μL aliquots for *S. aureus* and 700 μL aliquots for *E. coli* at 0, 15, 30, 45, 60, and 90 min post-irradiation. The *S. aureus* samples were analyzed using the drop-seeding method, with the viable cell count expressed as log CFU mL^{-1}. For *E. coli*, bioluminescence was measured using a TD-20/20 luminometer with a detection range of 300–650 nm and a peak wavelength of 420 nm, and results were reported as log RLU. At least three independent assays were performed for each condition, with two replicates for each assay.

3.5.4. Cytotoxicity assays

The Vero cell line (ECACC 88020401, African green monkey kidney cells, clone GMK) was utilized following the International Organization for Standardization (ISO) guidelines (ISO 10993–5). These cells were cultured in Dulbecco's Modified Eagle Medium (DMEM), supplemented with 100 U mL^{-1} penicillin, 100 μg mL^{-1} streptomycin, 0.25 μg mL^{-1} amphotericin B and 10 % (v/v) fetal bovine serum (FBS).

The Vero cells were plated at a density of 9.4×10^4 cells cm^{-2} in 96-well plates culture and incubated overnight in a medium under a 5 % CO_2 atmosphere. Following this, the cells were washed twice with PBS and treated with DMEM solutions containing porphyrin-based PS at concentrations of 0.5, 1.0, and 5.0 μM for 24 h in an incubator with 95 % air and 5 % CO_2. To evaluate cell viability after PS treatment, the reduction of the sodium salt of 7-hydroxy-3H-phenoxazine-3-one-10-oxide (Resazurin) to resorufin was measured using a SynergyTM HT Multi-Detection microplate reader. The data were reported as a percentage relative to the control, which was determined by the optical density (OD) of resorufin at 570 nm from untreated cells. The study included three independent experiments, each conducted in triplicate.

3.5.5. Statistical analysis

Statistical analysis was carried out using GraphPad Prism 8. Normal distribution was verified using the Kolmogorov-Smirnov test, and variance homogeneity was evaluated with the Brown-Forsythe test. For evaluating PS cell adhesion, one-way ANOVA was used to analyze the differences in PS concentrations bound to bacterial cells, with subsequent comparisons made using Tukey's and Dunnett's tests. In the case of photodynamic inactivation assays, two-way ANOVA was employed to compare bacterial concentrations between samples and controls at various time points, followed by post-hoc analyses using Tukey's test. A *p*-value of less than 0.05 was deemed statistically significant.

4. Conclusions

In summary, these studies demonstrated that the coordination of the metal ions Zn(II), Co(II) and Pd(II) within the porphyrin-triphenylphosphonium core significantly affected the photophysical, photochemical and photodynamic features of the resulting complexes. While coordination of porphyrin **1** with Zn(II) did not substantially impact its emission or ability to generate $^1O_2$, the corresponding Pd(II) and Co(II) complexes became non-emissive in PBS and were unable to generate significative $^1O_2$ in DMF. The results suggest that, for these two metalloporphyrins, the decay to the ground state after excitation occurs mainly through non-radiative pathways. Although further efforts and improvements are required to enhance the (photo)stability of the Zn(II) porphyrin-triphenylphosphonium complexes **1-Zn**, **2-Zn** and **3-Zn**, the results demonstrated promising potential as suitable PS for photodynamic applications.

The photodynamic efficiencies of this series of cationic metalloporphyrins with triphenylphosphonium units against Gram-positive MRSA and Gram-negative *E. coli* revealed that Pd(II) and Co(II) complexes completely failed to photoinactivate both MRSA and *E. coli* bacterial strains. This is likely due to their higher tendency to aggregate and their inability to efficiently generate ROS, namely $^1O_2$. In contrast, Zn(II)-based metalloporphyrins demonstrated more promising results and their better effectiveness can be related to their better bacterial cell adhesion, as well as good ability to generate $^1O_2$. The photodynamic assays highlighted that the metalloporphyrin **2-Zn**, containing three triphenylphosphonium moieties and six positive charges, was especially effective as PS. This underscores the importance of fine-tuning the structural features of porphyrins to develop efficient PS for aPDT. A well-balanced chemical structure that includes the appropriate number of triphenylphosphonium units, a Zn(II) ion at the porphyrin core, and

an electron-withdrawing pentafluorophenyl unit, made metalloporphyrin **2-Zn** a standout PS. This PS outperformed the activity of its free-base counterpart, particularly at lower concentrations, and was highly effective in the photoinactivation of *E. coli*, allowing for a concentration reduction from 5.0 μM to 1.0 μM while reducing irradiation time by more than 66 %.

These findings, along with the absence of cytotoxicity in host cells, indicate that porphyrin-triphenylphosphonium metal complexes, namely with Zn(II), hold great potential and can play an important role in the development of efficient PS for addressing the growing issue of antibiotic-resistant bacteria, with applications in both clinical and environmental fields.

CRediT authorship contribution statement

Inês Chaves: Writing – original draft, Investigation. **Filipe F.M. Morais:** Investigation. **Cátia Vieira:** Writing – original draft, Investigation, Formal analysis. **Maria Bartolomeu:** Investigation. **Ana T.P.C. Gomes:** Writing – review & editing. **M. Amparo F. Faustino:** Writing – review & editing, Validation. **M. Graça P.M.S. Neves:** Writing – review & editing, Validation. **Adelaide Almeida:** Writing – review & editing, Supervision, Methodology. **Nuno M.M. Moura:** Writing – review & editing, Writing – original draft, Supervision, Methodology, Conceptualization.

Funding

This research work received financial support from the University of Aveiro and FCT/MCTES to support the https://doi.org/10.54499/LA/P/0008/2020 https://doi.org/10.54499/UIDP/50006/2020UID/50006 -Laboratório Associado para a Química Verde - Tecnologias e Processos Limposhttps://doi.org/10.54499/UIDB/50006/2020) and UID Centro de Estudos do Ambiente e Mar (CESAM) + LA/P/0094/2020 research units through national funds and, where applicable, was co-financed by the FEDER, within the PT2020 Partnership Agreement, and to the Portuguese NMR Network. The NMR spectrometers are part of the National NMR Network (PTNMR) and are partially supported by Infrastructure Project N° 022161 (co-financed by FEDER through COMPETE 2020, POCI and PORL and FCT through PIDDAC). This work was developed within the project PORP2PS (EXPL/QUIQOR/0586/2021), financially supported by national funds (OE) through FCT/MCTES. This research was also funded by FCT through the financial support of the Centre for Interdisciplinary Research in Health (CIIS) under the Strategic Project Nos. UIDB/04279/2020 and UIDP/04279/2020. FMP Morais thanks FCT for his PhD Grant (UI/BD/154486/2022). This research was also funded by FCT and UCP through the CEEC institutional financing of ATPC Gomes (CEECINST/00137/2018/CP1520/CT0022). NMM Moura gratefully acknowledges FCT for an Assistant Research Position through program CEECIND6 – Individual Call to Scientific Employment Stimulus 6th Edition (2023.06495.CEECIND).

Declaration of competing interest

The authors declare that they have no known competing financial interests or personal relationships that could have appeared to influence the work reported in this paper.

Acknowledgements

The authors thank the University of Aveiro and Fundação para a Ciência e Tecnologia and Ministério da Ciência, Tecnologia e Ensino Superior (FCT/MCTES) for financial support to LAQV-REQUIMTE (UID/50006 research units, and Portuguese NMR Network. “The NMR spectrometers are part of the National NMR Network (PTNMR) and are partially supported by Infrastructure Project N° 022161 (co-financed by FEDER through COMPETE 2020, POCI and PORL and FCT through PIDDAC).

Appendix A. Supplementary material

Supplementary data to this article can be found online at https://doi.org/10.1016/j.inoche.2025.114426.

Data availability

Data will be made available on request.

References

[1] M.I. Hutchings, A.W. Truman, B. Wilkinson, Antibiotics: past, present and future, Curr. Opin. Microbiol. 51 (2019) 72–80, https://doi.org/10.1016/j.mib.2019.10.008.
[2] N. Waglechner, G.D. Wright, Antibiotic resistance: it’s bad, but why isn’t it worse? BMC Biol. 15 (2017) 84, https://doi.org/10.1186/s12915-017-0423-1.
[3] C. Hobson, A.N. Chan, G.D. Wright, The antibiotic resistome: a guide for the discovery of natural products as antimicrobial agents, Chem. Rev. 121 (2021) 3464–3494, https://doi.org/10.1021/acs.chemrev.0c01214.
[4] M.R. Milenković, V. Živković-Radovanović, L. Andjelković, Synthesis and antimicrobial activity of (3-formyl-4-hydroxybenzyl)triphenylphosphonium chloride acylhydrazones, Russ. J. Gen. Chem. 90 (2020) 1716–1720, https://doi.org/10.1134/S1070363220090194.
[5] X. Moreira, P. Santos, M.A.F. Faustino, M.M.M. Raposo, S.P.G. Costa, N.M. M. Moura, A.T.P.C. Gomes, A. Almeida, M.G.P.M.S. Neves, An insight into the synthesis of cationic porphyrin-imidazole derivatives and their photodynamic inactivation efficiency against Escherichia coli, Dyes Pigm. 178 (2020) 108330, https://doi.org/10.1016/j.dyepig.2020.108330.
[6] B. Amos-Tautua, S. Songca, O. Oluwafemi, Application of porphyrins in antibacterial photodynamic therapy, Molecules 24 (2019) 2456, https://doi.org/10.3390/molecules24132456.
[7] R. Bresolí-Obach, I. Gispert, D.G. Peña, S. Boga, Ó. Gulias, M. Agut, M.E. Vázquez, S. Nonell, Triphenylphosphonium cation: a valuable functional group for antimicrobial photodynamic therapy, J. Biophotonics 11 (2018) e201800054, https://doi.org/10.1002/jbio.201800054.
[8] F. Sperandio, Y.-Y. Huang, M. Hamblin, Antimicrobial photodynamic therapy to kill gram-negative bacteria, Recent Pat. Antiinfect. Drug Discov. 8 (2013) 108–120, https://doi.org/10.2174/1574891x113089990012.
[9] N. Fotinos, M. Convert, J.-C. Piffaretti, R. Gurny, N. Lange, Effects on Gram-Negative and Gram-Positive bacteria mediated by 5-aminolevulinic acid and 5-aminolevulinic acid derivatives, Antimicrob. Agents Chemother. 52 (2008) 1366–1373, https://doi.org/10.1128/AAC.01372-07.
[10] C. Vieira, A.T.P.C. Gomes, M.Q. Mesquita, N.M.M. Moura, M.G.P.M.S. Neves, M.A. F. Faustino, A. Almeida, An insight into the potentiation effect of potassium iodide on aPDT efficacy, Front. Microbiol. 9 (2018) 2665, https://doi.org/10.3389/fmicb.2018.02665.
[11] M. Klausen, M. Ucuncu, M. Bradley, Design of photosensitizing agents for targeted antimicrobial photodynamic therapy, Molecules 25 (2020) 5239, https://doi.org/10.3390/molecules25225239.
[12] N. Kashef, Y.-Y.-Y. Huang, M.R. Hamblin, Advances in Antimicrobial Photodynamic Inactivation at the Nanoscale, Walter De Gruyter GmbH, 2017 doi: 10.1515/nanoph-2016-0189.
[13] M.R. Hamblin, Antimicrobial photodynamic inactivation: a bright new technique to kill resistant microbes, Curr. Opin. Microbiol. 33 (2016) 67–73, https://doi.org/10.1016/j.mib.2016.06.008.
[14] M.T. Islam, M. Sain, C. Stark, M. Fefer, J. Liu, T. Hoare, W. Ckurshumova, C. Rosa, Overview of methods and considerations for the photodynamic inactivation of microorganisms for agricultural applications, Photochem. Photobiol. Sci. 22 (2023) 2675–2686, https://doi.org/10.1007/s43630-023-00466-6.
[15] E. Dube, G.E. Okuthe, Applications of antimicrobial photodynamic therapy in aquaculture: effect on fish pathogenic bacteria, Fishes 9 (2024) 99, https://doi.org/10.3390/fishes9030099.
[16] E. Alves, M.A.F. Faustino, M.G.P.M.S. Neves, Â. Cunha, H. Nadais, A. Almeida, Potential applications of porphyrins in photodynamic inactivation beyond the medical scope, J. Photochem. Photobiol. C: Photochem. Rev. 22 (2015) 34–57, https://doi.org/10.1016/j.jphotochemrev.2014.09.003.
[17] M.Q. Mesquita, C.J. Dias, M.G.P.M.S. Neves, A. Almeida, M.A.F. Faustino, Revisiting current photoactive materials for antimicrobial photodynamic therapy, Molecules 23 (2018) 2424, https://doi.org/10.3390/molecules23102424.
[18] L. Sobotta, P. Skupin-Mrugalska, J. Piskorz, J. Mielcarek, Porphyrinoid photosensitizers mediated photodynamic inactivation against bacteria, Eur. J. Med. Chem. 175 (2019) 72–106, https://doi.org/10.1016/j.ejmech.2019.04.057.
[19] F. Cieplik, D. Deng, W. Crielaard, W. Buchalla, E. Hellwig, A. Al-Ahmad, T. Maisch, Antimicrobial photodynamic therapy – what we know and what we don’t, Crit. Rev. Microbiol. 44 (2018) 571–589, https://doi.org/10.1080/1040841X.2018.1467876.
[20] H. Abrahamse, M.R. Hamblin, New photosensitizers for photodynamic therapy, Biochem. J. 473 (2017) 347–364, https://doi.org/10.1042/BJ20150942.New.

[21] B. Yang, Y. Chen, J. Shi, Reactive Oxygen Species (ROS)-based nanomedicine, Chem. Rev. 119 (2019) 4881–4985, https://doi.org/10.1021/acs.chemrev.8b00626.

[22] E.H. Morales, C.A. Pinto, R. Luraschi, C.M. Muñoz-Villagrán, F.A. Cornejo, S. W. Simpkins, J. Nelson, F.A. Arenas, J.S. Piotrowski, C.L. Myers, H. Mori, C. C. Vásquez, Accumulation of heme biosynthetic intermediates contributes to the antibacterial action of the metalloid tellurite, Nat. Commun. 8 (2017) 15320, https://doi.org/10.1038/ncomms15320.

[23] E. Alves, M.A.F. Faustino, M.G.PM.S. Neves, A. Cunha, J.P.C. Tomé, A. Almeida, An insight on bacterial cellular targets of photodynamic inactivation, Future Med. Chem. 6 (2014) 141–164, https://doi.org/10.4155/fmc.13.211.

[24] M.Q. Mesquita, C.J. Dias, M.G.P.M.S. Neves, A. Almeida, M.A.F. Faustino, The role of photoactive materials based on tetrapyrrolic macrocycles in antimicrobial photodynamic therapy, in: Handb. Porphyr. Sci., World Scientific Publishing Co., Singapore, 2022, pp. 201–277, https://doi.org/10.1142/9789811246760_0221.

[25] I.O. Savelyeva, K.A. Zhdanova, M.A. Gradova, O.V. Gradov, N.A. Bragina, Cationic porphyrins as antimicrobial and antiviral agents in photodynamic therapy, Curr. Issues Mol. Biol. 45 (2023) 9793–9822, https://doi.org/10.3390/cimb45120612.

[26] M. Grimmeisen, C. Jessen-Trefzer, Increasing the selectivity of light-active antimicrobial agents – or how to get a photosensitizer to the desired target, Chembiochem 24 (2023) e202300177, https://doi.org/10.1002/cbic.202300177.

[27] W. Zhou, X. Jiang, X. Zhen, Development of organic photosensitizers for antimicrobial photodynamic therapy, Biomater. Sci. 11 (2023) 5108–5128, https://doi.org/10.1039/D3BM00730H.

[28] A. Akbar, S. Khan, T. Chatterjee, M. Ghosh, Unleashing the power of porphyrin photosensitizers: illuminating breakthroughs in photodynamic therapy, J. Photochem. Photobiol. B Biol. 248 (2023) 112796, https://doi.org/10.1016/j.jphotobiol.2023.112796.

[29] A. Galstyan, Y.K. Maurya, H. Zhylitskaya, Y.J.WuY. Bae, M.R. Wasielewski, T. Lis, U. Dobrindt, M. Stępień, π-extended donor–acceptor porphyrins and metalloporphyrins for antimicrobial photodynamic inactivation, Chem. Eur. J. 26 (37) (2020) 8262–8266, https://doi.org/10.1002/chem.201905372.

[30] E.S. Nyman, P.H. Hynninen, Research advances in the use of tetrapyrrolic photosensitizers for photodynamic therapy, J. Photochem. Photobiol. B Biol. 73 (2004) 1–28, https://doi.org/10.1016/j.jphotobiol.2003.10.002.

[31] E. Paszko, C. Ehrhardt, M.O. Senge, D.P. Kelleher, J.V. Reynolds, Nanodrug applications in photodynamic therapy, Photodiagn. Photodyn. Ther. 8 (2011) 14–29, https://doi.org/10.1016/j.pdpdt.2010.12.001.

[32] K.M. Kadish, K.M. Smith, R. Guilard, Handbook of Porphyrin Science, World Scientific Publishing Company, Singapore, 2010.

[33] G. Singh, S. Chandra, Unravelling the structural-property relations of porphyrinoids with respect to photo- and electro-chemical activities, Electrochem. Sci. Adv. 3 (2023) e2100149, https://doi.org/10.1002/elsa:202100149.

[34] Y. Ding, W.-H.-H. Zhu, Y. Xie, Development of ion chemosensors based on porphyrin analogues, Chem. Rev. 117 (2017) 2203–2256, https://doi.org/10.1021/acs.chemrev.6b00021.

[35] W. Zhang, W. Lai, R. Cao, Energy-related small molecule activation reactions: oxygen reduction and hydrogen and oxygen evolution reactions catalyzed by porphyrin- and corrole-based systems, Chem. Rev. 117 (2017) 3717–3797, https://doi.org/10.1021/acs.chemrev.6b00299.

[36] S. Hiroto, Y. Miyake, H. Shinokubo, Synthesis and functionalization of porphyrins through organometallic methodologies, Chem. Rev. 117 (2017) 2910–3043, https://doi.org/10.1021/acs.chemrev.6b00427.

[37] R. Paolesse, S. Nardis, D. Monti, M. Stefanelli, C. Di Natale, Porphyrinoids for chemical sensor applications, Chem. Rev. 117 (2017) 2517–2583, https://doi.org/10.1021/acs.chemrev.6b00361.

[38] M. Urbani, M. Grätzel, M.K. Nazeeruddin, T. Torres, Meso-substituted porphyrins for dye-sensitized solar cells, Chem. Rev. 114 (2014) 12330–12396, https://doi.org/10.1021/cr5001964.

[39] M. Imran, M. Ramzan, A. Qureshi, M. Khan, M. Tariq, Emerging applications of porphyrins and metalloporphyrins in biomedicine and diagnostic magnetic resonance imaging, Biosensors 8 (2018) 95, https://doi.org/10.3390/bios8040095.

[40] I.A. Abdulaeva, K.P. Birin, A. Bessmertnykh-Lemeune, A.Y. Tsivadze, Y. G. Gorbunova, Heterocycle-appended porphyrins: synthesis and challenges, Coord. Chem. Rev. 407 (2020) 213108, https://doi.org/10.1016/j.ccr.2019.213108.

[41] Y. Kuramochi, A. Satake, Metalloporphyrins: their multitalented nature as observed in multi-metal complex systems, Dalt. Trans. 52 (2023) 5418–5422, https://doi.org/10.1039/D2DT04104A.

[42] K. Kalyanasundaram, M. Grätzel, Applications of functionalized transition metal complexes in photonic and optoelectronic devices, Coord. Chem. Rev. 177 (1998) 347–414, https://doi.org/10.1016/S0010-8545(98)00189-1.

[43] H. Huang, W. Song, J. Rieffel, J.F. Lovell, Emerging applications of porphyrins in photomedicine, Front. Phys. 3 (2015), https://doi.org/10.3389/fphy.2015.00023.

[44] L. Zou, R. Sa, H. Lv, H. Zhong, R. Wang, Recent advances on metalloporphyrin-based materials for visible-light-driven CO 2 reduction, ChemSusChem 13 (2020) 6124–6140, https://doi.org/10.1002/cssc.202001796.

[45] P. Sarbadhikary, B.P. George, H. Abrahamse, Recent advances in photosensitizers as multifunctional theranostic agents for imaging-guided photodynamic therapy of cancer, Theranostics. 11 (2021) 9054–9088, https://doi.org/10.7150/thno.62479.

[46] J.S. O'Neill, L. Kearney, M.P. Brandon, M.T. Pryce, Design components of porphyrin-based photocatalytic hydrogen evolution systems: a review, Coord. Chem. Rev. 467 (2022) 214599, https://doi.org/10.1016/j.ccr.2022.214599.

[47] J.M. Park, K.-I. Hong, H. Lee, W.-D. Jang, Bioinspired applications of porphyrin derivatives, Acc. Chem. Res. 54 (2021) 2249–2260, https://doi.org/10.1021/acs.accounts.1c00114.

[48] L.M. Moreira, F. Vieira dos Santos, J.P. Lyon, M. Maftoum-Costa, C. Pacheco-Soares, N. Soares da Silva, Photodynamic therapy: porphyrins and phthalocyanines as photosensitizers, Aust. J. Chem. 61 (2008) 741–754, https://doi.org/10.1071/CH08145.

[49] T.H.S. Souza, J.F. Sarmento-Neto, S.O. Souza, B.L. Raposo, B.P. Silva, C.P. F. Borges, B.S. Santos, P.E. Cabral Filho, J.S. Rebouças, A. Fontes, Advances on antimicrobial photodynamic inactivation mediated by Zn(II) porphyrins, J. Photochem. Photobiol. C: Photochem. Rev. 49 (2021) 100454, https://doi.org/10.1016/j.jphotochemrev.2021.100454.

[50] R. Chandra, M. Tiwari, P. Kaur, M. Sharma, R. Jain, S. Dass, Metalloporphyrins—applications and clinical significance, Indian J. Clin. Biochem. 15 (2000) 183–199, https://doi.org/10.1007/bf02867558.

[51] J.M.D. Calmeiro, S.R.D. Gamelas, A.T.P.C. Gomes, M.A.F. Faustino, M.G.P.M. S. Neves, A. Almeida, J.P.C. Tomé, L.M.O. Lourenço, Versatile thiopyridyl/pyridinone porphyrins combined with potassium iodide and thiopyridinium/methoxypyridinium porphyrins on E. coli photoinactivation, Dyes Pigm. 181 (2020), https://doi.org/10.1016/j.dyepig.2020.108476.

[52] B. Pucelik, A. Barzowska, A. Sułek, M. Werłos, J.M. Dąbrowski, Refining antimicrobial photodynamic therapy: effect of charge distribution and central metal ion in fluorinated porphyrins on effective control of planktonic and biofilm bacterial forms, Photochem. Photobiol. Sci. 23 (2024) 539–560, https://doi.org/10.1007/s43630-024-00538-1.

[53] B.B. Beyene, G.A. Wassie, Antibacterial activity of Cu(II) and Co(II) porphyrins: role of ligand modification, BMC Chem. 14 (2020) 51, https://doi.org/10.1186/s13065-020-00701-6.

[54] I. Chaves, F.M.P. Morais, C. Vieira, M. Bartolomeu, M.A.F. Faustino, M.G.P.M. S. Neves, A. Almeida, N.M.M. Moura, Can porphyrin–triphenylphosphonium conjugates enhance the photosensitizer performance toward bacterial strains? ACS Appl. Bio Mater. 7 (2024) 5541–5552, https://doi.org/10.1021/acsabm.4c00659.

[55] A. Maraval, S. Franco, C. Vialas, G. Pratviel, M.A. Blasco, B. Meunier, Porphyrin–aminoquinoline conjugates as telomerase inhibitors, Org. Biomol. Chem. 1 (2003) 921–927, https://doi.org/10.1039/B211634K.

[56] M.C.S. Vallejo, M.J.A. Reis, A.M.V.M. Pereira, V.V. Serra, J.A.S. Cavaleiro, N.M. M. Moura, M.G.P.M.S. Neves, Merging pyridine(s) with porphyrins and analogues: an overview of synthetic approaches, Dyes Pigm. 191 (2021) 109298, https://doi.org/10.1016/j.dyepig.2021.109298.

[57] N.M.M. Moura, S. Guedes, D. Salvador, H. Oliveira, M.Q. Alves, N. Paradis, C. Wu, M.G.P.M.S. Neves, C.I.V. Ramos, Oncogenic and telomeric G-quadruplexes: targets for porphyrin-triphenylphosphonium conjugates, Int. J. Biol. Macromol. 277 (2024) 134126, https://doi.org/10.1016/j.ijbiomac.2024.134126.

[58] W. Zheng, N. Shan, L. Yu, X. Wang, UV-visible, fluorescence and EPR properties of porphyrins and metalloporphyrins, Dyes Pigm. 77 (2008) 153–157, https://doi.org/10.1016/j.dyepig.2007.04.007.

[59] L.G. Arnaut, Design of porphyrin-based photosensitizers for photodynamic therapy, Adv. Inorg. Chem. (2011) 187–233, https://doi.org/10.1016/B978-0-12-385904-4.00006-8.

[60] W. Wu, B. Liu, Aggregation-induced emission: challenges and opportunities, Natl. Sci. Rev. 8 (2021) 8–10, https://doi.org/10.1093/nsr/nwaa222.

[61] T. Entradas, S. Waldron, M. Volk, The detection sensitivity of commonly used singlet oxygen probes in aqueous environments, J. Photochem. Photobiol. B Biol. 204 (2020) 111787, https://doi.org/10.1016/j.jphotobiol.2020.111787.

[62] E. Zenkevich, E. Sagun, V. Knyukshto, A. Shulga, A. Mironov, O. Efremova, R. Bonnett, S.P. Songca, M. Kassem, Photophysical and photochemical properties of potential porphyrin and chlorin photosensitizers for PDT, J. Photochem. Photobiol. B Biol. 33 (1996) 171–180, https://doi.org/10.1016/1011-1344(95)07241-1.

[63] W. Spiller, H. Kliesch, D. Wöhrle, S. Hackbarth, B. Röder, G. Schnurpfeil, Singlet oxygen quantum yields of different photosensitizers in polar solvents and micellar solutions, J. Porphyrins Phthalocyanines. 2 (1998) 145–158, https://doi.org/10.1002/(SICI)1099-1409(199803/04)2:2<145::AID-JPP60>3.0.CO;2-2.

[64] A. Garcia-Sampedro, A. Tabero, I. Mahamed, P. Acedo, Multimodal use of the porphyrin TMPyP: from cancer therapy to antimicrobial applications, J. Porphyrins Phthalocyanines 23 (2019) 11–27, https://doi.org/10.1142/s1088424619500111.

[65] N. Kumar, V. Roopa, M.K. Bhalla, Beyond zinc coordination: bioimaging applications of Zn(II)-complexes, Coord. Chem. Rev. 427 (2021) 213550, https://doi.org/10.1016/j.ccr.2020.213550.

[66] W.M. Leevy, S.T. Gammon, H. Jiang, J.R. Johnson, D.J. Maxwell, E.N. Jackson, M. Marquez, D. Piwnica-Worms, B.D. Smith, Optical imaging of bacterial infection in living mice using a fluorescent near-infrared molecular probe, J. Am. Chem. Soc. 128 (2006) 16476–16477, https://doi.org/10.1021/ja0665592.

[67] I. Kurvet, A. Ivask, O. Bondarenko, M. Sihtmäe, A. Kahru, LuxCDABE—transformed constitutively bioluminescent Escherichia coli for toxicity screening: comparison with naturally luminous Vibrio fischeri, Sensors 11 (2011) 7865–7878, https://doi.org/10.3390/s110807865.

[68] S. George, M.R. Hamblin, A. Kishen, Uptake pathways of anionic and cationic photosensitizers into bacteria, Photochem. Photobiol. Sci. 8 (2009) 788–795, https://doi.org/10.1039/b809624d.

[69] P.S.S. Lacerda, M. Bartolomeu, A.T.P.C. Gomes, A.S. Duarte, A. Almeida, M.A. F. Faustino, M.G.P.M.S. Neves, J.F.B. Barata, Can corrole dimers be good photosensitizers to kill bacteria? Microorganisms. 10 (2022) 1167 https://doi.org/10.3390/microorganisms10061167.

[70] L. Marciel, M.Q. Mesquita, R. Ferreira, B. Moreira, M.G.P.M.S. Neves, M.A. F. Faustino, A. Almeida, An efficient formulation based on cationic porphyrins to photoinactivate Staphylococcus aureus and Escherichia coli, Future Med. Chem. 10 (2018) 1821–1833, https://doi.org/10.4155/fmc-2018-0010.

[71] Q. Lei, X. Lai, Y. Zhang, Z. Li, R. Li, W. Zhang, N. Ao, H. Zhang, PEGylated bis-quaternary triphenyl-phosphonium tosylate allows for balanced antibacterial activity and cytotoxicity, ACS Appl. Bio Mater. 3 (2020) 6400–6407, https://doi.org/10.1021/acsabm.0c00837.

[72] P. Kubát, K. Lang, P. Anzenbacher Jr, K. Jursíková, V. Král, B. Ehrenberg, Interaction of novel cationic meso-tetraphenylporphyrins in the ground and excited states with DNA and nucleotides, J. Chem. Soc. Perkin Trans. 1 (2000) 933–941, https://doi.org/10.1039/a909466k.

[73] N.M.M. Moura, J.A.S. Cavaleiro, M.G.P.M.S. Neves, C.I.V. Ramos, opp-Dibenzoporphyrin pyridinium derivatives as potential G-quadruplex DNA ligands, Molecules 28 (2023) 6318, https://doi.org/10.3390/molecules28176318.

[74] M. Bartolomeu, S. Rocha, Â. Cunha, M.G.P.M.S. Neves, M.A.F. Faustino, A. Almeida, Effect of photodynamic therapy on the virulence factors of Staphylococcus aureus, Front. Microbiol. 7 (2016) 267, https://doi.org/10.3389/fmicb.2016.00267.

[75] E. Alves, C.M.B. Carvalho, J.P.C. Tomé, M.A.F. Faustino, M.G.P.M.S. Neves, A. C. Tomé, J.A.S. Cavaleiro, Â. Cunha, S. Mendo, A. Almeida, Photodynamic inactivation of recombinant bioluminescent *Escherichia coli* by cationic porphyrins under artificial and solar irradiation, J. Ind. Microbiol. Biotechnol. 35 (2008) 1447–1454, https://doi.org/10.1007/s10295-008-0446-2.

[76] C. Vieira, A. Santos, M.Q. Mesquita, A.T.P.C. Gomes, M.G.P.M.S. Neves, M.A. F. Faustino, A. Almeida, Advances in aPDT based on the combination of a porphyrinic formulation with potassium iodide: effectiveness on bacteria and fungi planktonic/biofilm forms and viruses, J. Porphyrins Phthalocyanines 23 (2019) 534–545, https://doi.org/10.1142/S1088424619500408.